Article

Cite This: *Biomacromolecules* 2019, 20, 3000−3008

pubs.acs.org/Biomac

Enzyme-Activatable Interferon−Poly(α-amino acid) Conjugates for Tumor Microenvironment Potentiation

Hao Wang,[†] Yingqin Hou,[†] Yali Hu,[†,‡] Jiaxiang Dou,[§] Youqing Shen,[∥] Yucai Wang,*[,§] and Hua Lu*[,†]

[†]Beijing National Laboratory for Molecular Sciences, Center for Soft Matter Science and Engineering, Key Laboratory of Polymer Chemistry and Physics of Ministry of Education, College of Chemistry and Molecular Engineering, and [‡]Peking-Tsinghua Center for Life Sciences, Academy for Advanced Interdisciplinary Studies, Peking University, Beijing 100871, China

[§]CAS Center for Excellence in Nanoscience, School of Life Sciences and Medical Center, University of Science and Technology of China, Hefei, Anhui 230027, China

[∥]Center for Bionanoengineering and Key Laboratory of Biomass Chemical Engineering of Ministry of Education, College of Chemical and Biological Engineering, Zhejiang University, Hangzhou 310027, China

Supporting Information

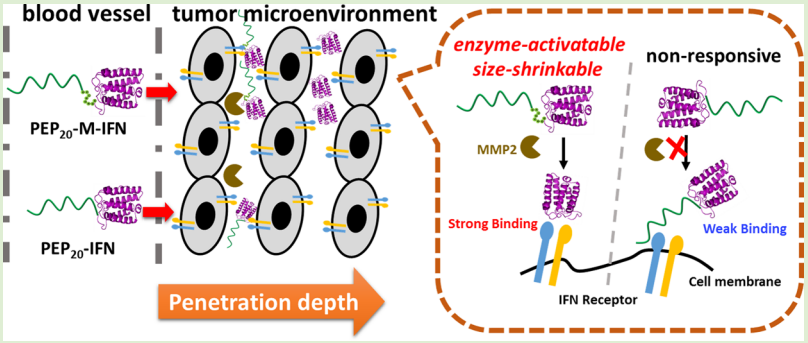

ABSTRACT: Protein−polymer conjugation is a clinically validated approach to enhanced pharmacokinetic properties. However, the permanent attachment of polymers often leads to irreversibly reduced protein bioactivity and poor tissue penetration. As such, the use of protein−polymer conjugates for solid tumors remains elusive. Herein, we report a simple strategy using enzyme-activatable and size-shrinkable protein−polypeptide conjugates to overcome this clinical challenge. Briefly, a matrix metalloproteinase (MMP)-responsive peptide sequence is introduced between a therapeutic protein interferon (IFN) and a synthetic polypeptide $P(EG_3Glu)_{20}$. The resulting site-specific MMP-responsive conjugate, denoted as PEP_{20}-M-IFN, can, therefore, release the attached $P(EG_3Glu)_{20}$ to achieve both protein activation and deep penetration into the tumor microenvironment (TME). Compared to a similarly produced nonresponsive analogue conjugate PEP_{20}-IFN, our results find PEP_{20}-M-IFN to show higher bioactivity in vitro, improved tumor retention, and deeper penetration in a MMP2-dependent manner. Moreover, systemic administration of PEP_{20}-M-IFN shows outstanding antitumor efficacy in both OVCAR3 and SKOV3 ovarian tumor models in mice. This work highlights the releasable PEPylation strategy for protein drug potentiation at the TME and opens up new opportunities in clinics for the treatment of malignant solid tumors.

INTRODUCTION

The development of therapeutic proteins has gained tremendous attention in recent years.[1−9] However, their clinical applications are severely impeded by several intrinsic limitations such as poor stability and short circulating half-life. Polymer modification of the protein-of-interest (e.g., PEGylation) is a proven strategy to improved pharmacokinetic (PK) profiles.[10−17] Presumably, the attachment of a polymer to the protein drug augments its overall hydrodynamic volume, leading to slower renal clearance and reduced immunogenicity. However, the conjugated polymers also create considerable steric hindrance undesirably blocking the interaction between the protein drug and its target, which eventually results in reduced efficacy in vivo, known as the "PEG dilemma".[18−20] For example, PEGASYS, a PEGylated interferon-α (IFN) currently used to treat hepatitis, retains only ∼7% biological activity of the pristine protein.[21] Poor tumor penetration is another notable drawback of PEGylation that draws growing attention recently. Indeed, none of the currently Food and Drug Administration-approved PEGylated proteins can treat solid tumors.[22] To overcome these limitations, continuous efforts have been devoted to the development of novel

Received: April 24, 2019
Revised: June 15, 2019
Published: July 16, 2019

DOI: 10.1021/acs.biomac.9b00560
Biomacromolecules 2019, 20, 3000−3008

Scheme 1. (A,B) Synthesis of the Two Conjugates: the MMP2-Activatable Conjugate PEP_{20}-M-IFN (A) and the Nonactivatable Conjugate PEP_{20}-IFN (B); (C) Cartoon Illustration of the Enzyme-Activation of PEP_{20}-M-IFN for Tumor Microenvironment Potentiation

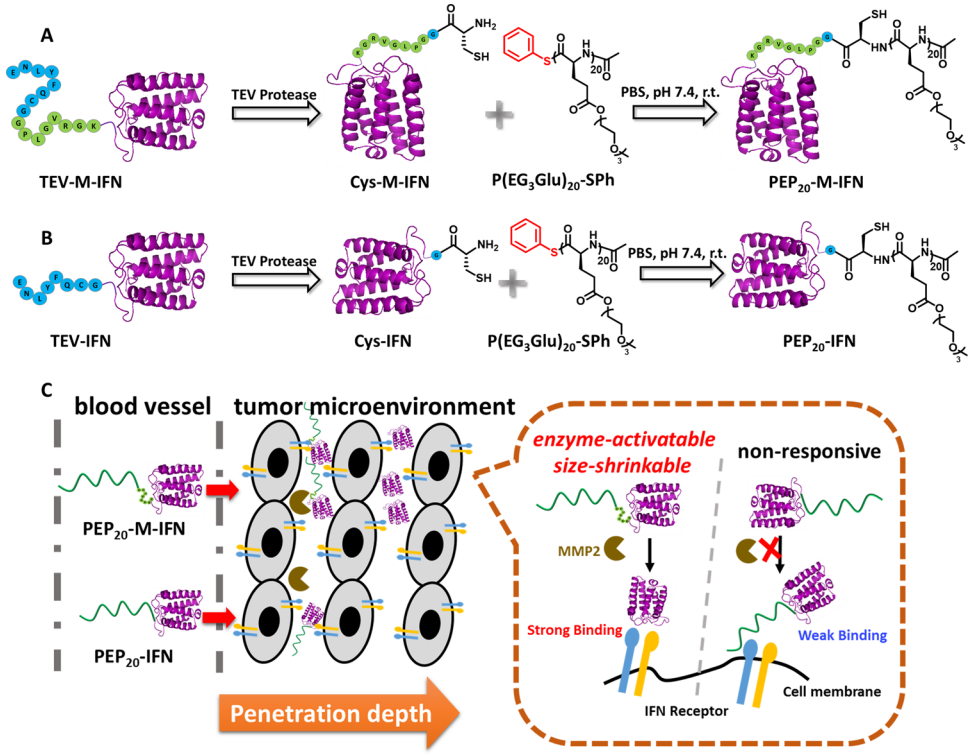

therapeutics simultaneously with optimized PK, efficacy, and deep tissue penetration for various solid tumors.

Recently, our group developed a technology termed as protein PEPylation, that is, the covalent modification of proteins with synthetic polypeptides [also known as poly(α-amino acid)].[23−27] Compared to the nondegradable PEG, polypeptides enjoy advantages such as biodegradability, broad chemical diversity, tunable physiochemical properties, and unique secondary structures.[28−37] We have shown that PEPylation can implement many beneficial properties including prolonged PK, greater efficacy, and significantly reduced immunogenicity,[38] compared to the traditional PEGylation. Moreover, by cyclizing the PEPylated conjugates, deep tumor penetration was enabled by the macrocyclic topology.[24] Nevertheless, the generation of the macrocyclic conjugates requires sophisticated knowledge in synthesis and purification.

Here, we present a releasable[39−44] strategy that leads to PEPylated proteins with enzymatically promoted activation and penetration. Matrix metalloproteinase (MMP) is a class of enzyme overexpressed in different types of tumors, which plays a critical role in tumor invasion and progression.[45,46] In the light of this, the designs of MMP-responsive delivering systems with improved penetration have received tremendous success in numerous nanomedicines.[47−55] Surprisingly, studies of using this approach in protein−polymer conjugates have been very rare.[19,56] We expect that the highly upregulated MMP2 in the tumor microenvironment (TME) can be harnessed to release the polymer from the protein, if a MMP-cleavable peptide sequence is inserted between the conjugated polymer and the protein-of-interest. Overall, the MMP-responsive protein conjugate is expected to gain sufficient long circulation and reduced systemic toxicity because of the conjugated polymer; once reaching the TME, the activity of the protein can be instantaneously restored to its full capacity due to the MMP-triggered polymer cleavage (Scheme 1). Moreover, we expect that the released protein can diffuse into deep tumor tissues by taking advantage of the smaller hydrodynamic size compared to the conjugate.[57−60] In this fashion, the present work may offer a simple but highly effective approach circumventing the long-standing PEG dilemma and allowing the treatment of solid tumors.

MATERIALS AND METHODS

Materials. 1,10-Phenanthroline (MMP inhibitor) was purchased from TCI (Tokyo, Japan). γ-(2-(2-(2-Methoxyethoxy)ethoxy)ethyl L-glutamate *N*-carboxyanhydride) ($EG_3GluNCA$) was produced according to an established protocol.[23] Human IFN-α enzyme-linked immunosorbent assay (ELISA) kit was obtained from Thermo (USA). All mice were purchased from Vital River Laboratories (Beijing, China). All animal experiments were performed in accordance with the local guidelines and with the approval from the Experimental Animal Ethics Committee in Beijing.

Protein Expression and Purification. The plasmid pET-TEV-M-IFN encoding recombinant human interferon alpha (IFN) tethered with a N-terminal ENLYFQCG*GPLGVRGK* and a C-terminal His_6 peptide tag was constructed and transformed into *Escherichia coli* BL21 cells. The pET-TEV-IFN plasmid encoding the IFN mutant without the MMP2-cleavable sequence (GPLGVRGK) was also produced in a similar method. The protein expression and purification were executed by following previously reported protocols with a maximum yield of 250 mg/L.[23]

Synthesis of PEP_{20}-M-IFN. PEP_{20}-M-IFN was prepared based on a previously reported protocol with slight modification.[24] Briefly, Cys-M-IFN (7.0 mg, 1.0 equiv) was concentrated in phosphate buffer saline (PBS) solution (pH 7.4) to ~7.0 mg/mL and then mixed with $P(EG_3Glu)_{20}$-SPh (Scheme 1A, 5.0 equiv). After the overnight

DOI: 10.1021/acs.biomac.9b00560
Biomacromolecules 2019, 20, 3000−3008

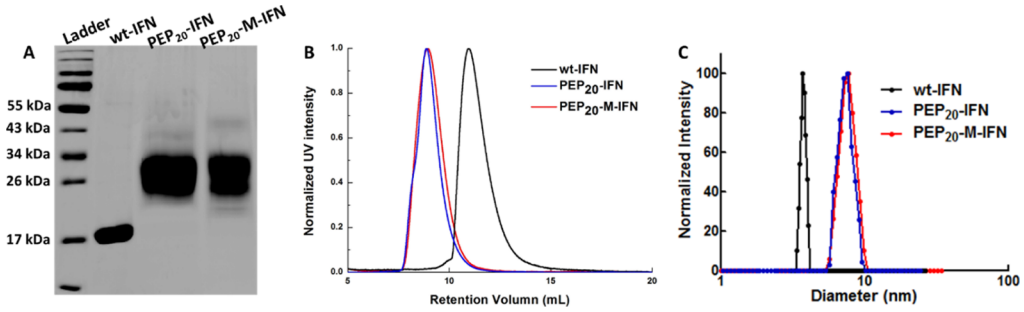

Figure 1. Characterization: (A) SDS-PAGE electrophoresis and (B) SEC of wt-IFN and the two conjugates. (C) DLS analysis of PEP_{20}-IFN and PEP_{20}-M-IFN in PBS buffer (pH 7.4).

incubation at 25 °C, the product PEP_{20}-M-IFN was purified via fast protein liquid chromatography on a size exclusion column with a yield ~67%.

DLS Measurement of the IFN Conjugates. The hydrodynamic diameters of the conjugates were measured on a Brookhaven NanoBrook Omni at room temperature. Because of the intrinsic tendency of IFN forming physical associates, samples were first passed through a size exclusion column in FPLC and used immediately for dynamic light scattering (DLS) analysis. The shear force during the size exclusion chromatography (SEC) process was found to destruct the physical associates of IFN temporarily.

MMP2 Cleavage of TEV-M-IFN and PEP_{20}-M-IFN. Daudi cells were seeded at a density of 4×10^5 cells/well in 6-well plates and incubated in opti-MEM for 24 h at 37 °C in 5% CO_2. The Daudi-conditioned MMP^+ media were collected, centrifuged, and incubated with TEV-M-IFN or PEP_{20}-M-IFN at 37 °C for different time periods. The cleavage by MMP2 was detected by using sodium dodecyl sulfate-polyacrylamide gel electrophoresis (SDS-PAGE) electrophoresis. The human umbilical vein endothelial cells (HUVEC)-conditioned medium was produced following a similar protocol and used as the MMP^- control.

In Vitro Cytotoxicity. Daudi cells were cultured in a 96-well plate (80 μL of 5000 cells per well) before the addition of various IFN drugs at gradient concentrations (20 μL, n = 3). After 72 h incubation, the cell proliferation inhibition was determined by CellTiter-Blue Viability Assay.

General Protocol for 5-TAMRA/FAM/Cy5-NHS or Cy5-Maleimide Labeling of wt-IFN or the IFN Conjugates. For the NHS-amine labeling, the IFN variant (1.0 mg, 1.0 equiv) was added to the dye-NHS (Cy5-NHS, FAM-NHS, or 5-TAMRA-NHS, 10.0 equiv), followed by reaction in PBS (pH 8.0) at 25 °C for 5 h. For the site-specific maleimide−thiol labeling, the IFN variant (1.0 mg, 1.0 equiv) was added to Cy5-maleimide (3.0 equiv), followed by reaction in PBS (pH 7.4) at 25 °C for 1 h. The dye-labeled products were purified with a PD 10 column in PBS (pH 7.4).

Flow Cytometry. Cy5 maleimide-labeled or FAM NHS-labeled PEP_{20}-M-IFN was incubated in the Daudi-conditioned MMP^+ media and then added to the Daudi cells at the final concentration of 90 μg/mL. After incubation for 1 h, the cells were centrifuged down, washed, and resuspended in PBS solution and further analyzed by flow cytometry. In the control experiment, dye-labeled PEP_{20}-M-IFN without the pretreatment of MMP^+ media was incubated with cells under the same conditions as described above.

Pharmacokinetics. The female Sprague-Dawley rats weighing ~250 g were randomly divided into three groups (n = 3) and injected with wt-IFN, PEP_{20}-IFN or PEP_{20}-M-IFN at a dose of 50 μg IFN/mouse through a jugular cannulated vein. At designated time points (1, 30 min, 1, 3, 6, 9, 12, 24, and 48 h), blood was withdrawn followed by centrifugation. The plasma IFN levels were evaluated by human IFN ELISA kit.

In Vivo Biodistribution. Female BALB/c nude mice (6-week old) were subcutaneously implanted with 1.0×10^7 SKOV-3 cells dispersed in 0.1 mL PBS. When the tumor size reached ~200−300 mm^3, the mice were randomly assigned to three groups (n = 3) and injected intravenously (i.v.) with Cy5-NHS labeled wt-IFN, PEP_{20}-IFN, or PEP_{20}-M-IFN at a dose of 30 μg IFN/mouse. The mice were imaged at predetermined time points (1.5, 3, 6, 9, 12, 24, and 48 h). The major organs and tumors were collected at 48 h and imaged by the In Vivo Imaging System.

In Vivo Tumor Penetration Study of IFN Conjugates w/o or with the MMP Inhibitor. Mice (n = 3) with ~200 mm^3 SKOV3 tumors were subcutaneously co-injected with Cy5 NHS-labeled PEP_{20}-M-IFN and 5-TAMRA-labeled PEP_{20}-IFN near the tumor site at a dose of 15 μg IFN for both conjugates. In parallel and in another group, the conjugates were co-injected at the same dosage 1 h after the intratumoral injection of 1,10-phenanthroline (10 mM, 50 μL). The mice were sacrificed 24 h after the IFN drug administration. Both tumor slices were stained with 4′,6-diamidino-2-phenylindole (DAPI) and imaged by confocal microscopy.

Ex Vivo Tumor Penetration Study of IFN Conjugates. SKOV3 tumors (~50 mm^3 in size) were extracted out and cocultured at room temperature with TAMRA-labeled PEP_{20}-IFN + Cy5-labeled PEP_{20}-M-IFN (0.09 mg/mL each) in $MMP2^+$ or $MMP2^-$ opti-MEM 0.20 mL for 24 h. To prepare the MMP^+ medium, a freshly extracted SKOV3 tumor (~500 mm^3 in size) was homogenized in opti-MEM (2.0 mL), followed by centrifugation to collect the supernatant.

In Vivo Antitumor Efficacy Using the OVCAR3 Model. The female BALB/c nude mice were s.c. implanted with 1.0×10^7 OVCAR3 cells dispersed in 0.2 mL mixture of RPMI 1640 medium/matrigel (v/v = 1:1). When the tumor size reached ~30 mm^3, (1.0 mL) mice were randomly assigned to four groups (n = 5−7). The tumor-bearing mice were i.v. administered with PBS saline, wt-IFN, PEP_{20}-IFN, or PEP_{20}-M-IFN every 5 days at a dosage of 20 μg IFN for eight times. Tumor volume was calculated by the following formula: $V = L \times W^2/2$, where L and W stand for the length and width of the tumor measured by an electronic caliper, respectively.

In Vivo Antitumor Efficacy Using the SKOV-3 Model. Female BALB/c nude mice (6-week old) were subcutaneously implanted with 1.0 × 107 SKOV-3 cells dispersed in 0.10 mL PBS. When the tumor size reached ~30 mm^3, mice were i.v. administered with PBS saline, wt-IFN, PEP_{20}-IFN, or PEP_{20}-M-IFN at a dosage of 20 μg IFN every 5 days. Each IFN per animal drug was administered four times.

Histopathology Evaluation. Mice of OVCAR3 model were sacrificed on day 27 after the treatment. The organs were collected, and then paraffin sections of tissues were stained with H&E for morphology observation.

RESULTS AND DISCUSSION

Synthesis and Characterization. To investigate the feasibility of the approach for solid tumors, IFN was selected as our model protein. The PEGylated IFN was previously used to treat indications such as melanoma and malignant skin lymphoma in clinics, but with limited success in treating other solid tumors such as ovarian cancers. We synthesized two conjugates according to our previously reported protocols (Scheme 1).[24] To prepare the suggested MMP2-activatable conjugates, we constructed a N-terminal fusion of interferon-

DOI: 10.1021/acs.biomac.9b00560
Biomacromolecules 2019, 20, 3000−3008

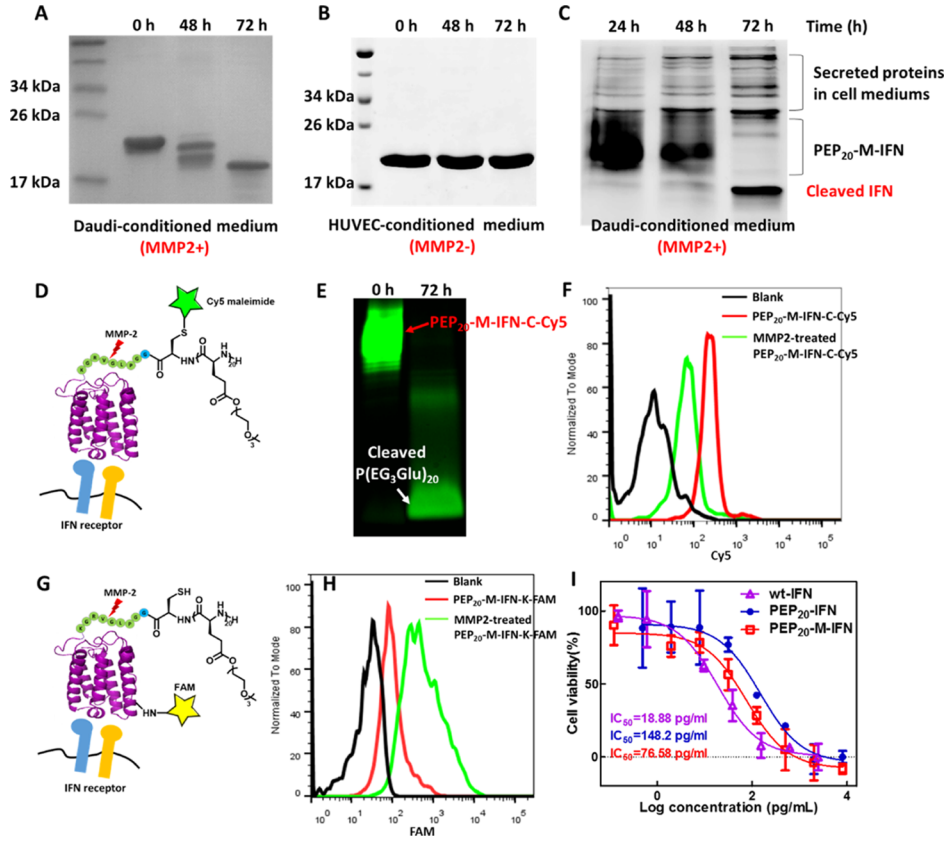

Figure 2. MMP2-dependent polymer cleavage and IFN activation. SDS-PAGE gel analysis of the enzyme cleavage of TEV-M-IFN in (A) $MMP2^+$ and (B) $MMP2^-$ media. (C) SDS-PAGE gel analysis of the enzyme cleavage of PEP_{20}-M-IFN in $MMP2^+$ medium. The gels were stained with Coomassie blue in (A–C). (D) Cartoon illustration of PEP_{20}-M-IFN-C-Cy5, the site-specific Cy5-labeled PEP_{20}-M-IFN through the thiol–maleimide chemistry. (E) Fluorescence imaging of the SDS-PAGE gel of PEP_{20}-M-IFN-C-Cy5 in $MMP2^+$ medium. (F) Flow cytometry analysis of PEP_{20}-M-IFN-C-Cy5 binding to Daudi cells with or without MMP2 pretreatment. (G) Cartoon illustration of PEP_{20}-M-IFN-K-FAM, the randomly FAM-labeled PEP_{20}-M-IFN through the NHS-amine chemistry. (H) Flow cytometry analysis of PEP_{20}-M-IFN-K-FAM binding to cells with or without pretreatment of MMP2. (I) Cytotoxicity of wt-IFN, PEP_{20}-IFN, and PEP_{20}-M-IFN against Daudi cells after 72 h incubation.

α2b denoted as TEV-M-IFN, which carried a TEV-cleavable sequence ENLYFQ⁝CG (⁝ indicates the cleavage site) and followed with a MMP2 substrate peptide GPLG⁝VRGK[61] (⁝ indicates the cleavage site) at the N-terminus of IFN (Scheme 1A). TEV-M-IFN was expressed in *E. coli* with a high expression yield of ~250 mg/L after optimization (Figure S1). To enable the site-specific PEPylation, TEV-M-IFN was first treated with TEV enzyme to obtain the IFN mutant bearing the N-terminal cysteine, Cys-M-IFN. Next, we prepared poly(γ-(2-(2-(2-methoxyethoxy)ethoxy)ethyl-L-glutamate) tethering a reactive phenyl thioester, denoted as $P(EG_3Glu)_{20}$-SPh, through the trimethylsilyl phenylsulfide-mediated ring-opening polymerization of α-amino acid *N*-carboxyanhydride (Figures S2 and S3).[26] Incubation of Cys-M-IFN and $P(EG_3Glu)_{20}$-SPh at room temperature yielded the N-terminal specific conjugate PEP_{20}-M-IFN via native chemical ligation. We also generated a control conjugate PEP_{20}-IFN having no MMP responsiveness by ligating $P(EG_3Glu)_{20}$-SPh to Cys-IFN as previously described (Scheme 1B). SDS-PAGE analysis confirmed the successful generation and narrow distribution of both conjugates with high purity (Figure 1A). SEC revealed that PEP_{20}-IFN and PEP_{20}-M-IFN had the same elution time, implying a similar hydrodynamic volume (Figure 1B). DLS measurement confirmed that PEP_{20}-IFN and PEP_{20}-M-IFN shared a similar diameter ~7.5 nm (Figure 1C).

MMP2-Dependent in Vitro Activation of PEP_{20}-M-IFN.

To investigate the MMP-specific cleavability, TEV-M-IFN was incubated with the Daudi cell-conditioned medium, which contained secreted MMP enzymes (MMP^+), and then analyzed by SDS-PAGE.[19] During the incubation, the band of TEV-M-IFN gradually disappeared in the SDS-PAGE gel, along with the appearance of a new band in the lower position corresponding to the cleaved wt-IFN (approximately 20 kDa) (Figure 2A). In contrast, TEV-IFN without the MMP-cleavable sequence showed no change under the same condition (Figure S4). Moreover, incubation of TEV-M-IFN with HUVEC cell-conditioned medium, which had no secreted MMP enzymes (MMP^-), showed negligible cleavage (Figure 2B). Collectively, these data validated the MMP-dependent cleavage for TEV-M-IFN, but not in TEV-IFN. With this success, we then moved on to test the MMP-mediated cleavage for the conjugate PEP_{20}-M-IFN. Incubation of PEP_{20}-M-IFN with MMP^+ medium showed a shift of the band to the lower position, similar to what was observed for TEV-M-IFN (Figure 2C). To further confirm the enzymatic cleavage, we labeled the conjugate site-specifically with one molecule of Cy5 through the maleimide–thiol reaction as shown in Figure 2D. Because the Cy5 was labeled before the MMP cleavage site, we expected a dimmed fluorescence for the IFN band after the MMP2 cleavage. Indeed, after incubation of the Cy5-labeled PEP_{20}-M-IFN (denoted as PEP_{20}-M-IFN-C-Cy5) with MMP^+

DOI: 10.1021/acs.biomac.9b00560
Biomacromolecules 2019, 20, 3000–3008

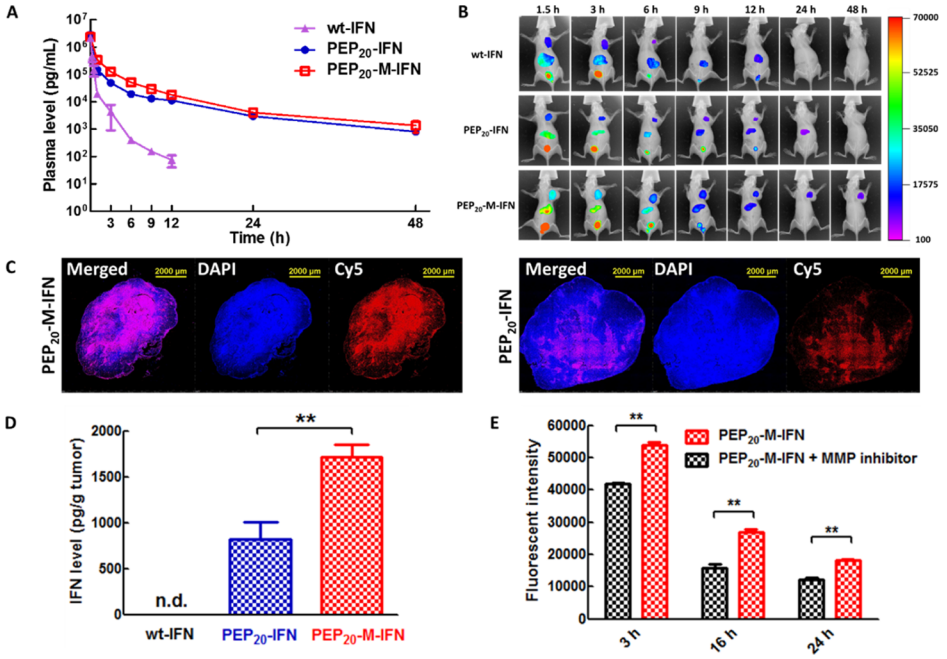

Figure 3. Pharmacokinetics and biodistribution. (A) Blood concentration of wt-IFN and the two conjugates at designated time points, measured by anti-IFN ELISA; Sprague-Dawley rats were infused with each IFN variant through tail vein and the blood was drawn from the cannulated jugular vein. (B) Fluorescence images of tumor-bearing mice at different time points after i.v. infusion of Cy5-labeled IFN variant. (C) Confocal images of the extracted tumor sections 48 h after i.v. infusion of Cy5-labeled PEP_{20}-M-IFN or PEP_{20}-IFN. (D) IFN concentrations in tumors 48 h after i.v. infusion, measured by anti-IFN ELISA. (E) Tumor accumulation of the locally administrated PEP_{20}-M-IFN at different time points with or without the pre-injection of the MMP inhibitor. Drugs were i.v. infused in (B–D) and subcutaneously injected nearby the tumor in (E). For studies in B–E, all the IFN samples were randomly labeled with Cy5 on the protein through the NHS-amine chemistry. Data are presented as mean ± standard deviation (SD); $^*P < 0.05$, $^{**}P < 0.01$ (*t*-test).

medium for 72 h, the fluorescence of the conjugate disappeared in the SDS-PAGE gel, whereas a new fluorescent band appeared at the bottom of the gel (less than 10 kDa), attributable to the cleaved $P(EG_3Glu)_{20}$ bearing the Cy5 dye (Figure 2E).

We further evaluated the binding affinity of the conjugates to the IFN receptor expressed on the surface of human cell membranes. Flow cytometry analysis revealed that PEP_{20}-M-IFN before enzyme activation had a similar binding affinity with PEP_{20}-IFN in various human cell lines including Daudi, OVCAR-3, and HUVEC cells (Figure S5). Interestingly, when PEP_{20}-M-IFN-C-Cy5 was pre-incubated with the $MMP2^+$ medium[19] before incubation with Daudi cells, the mean fluorescent intensity (MFI) in the flow cytometry was significantly reduced as compared to the one without MMP2 treatment (Figure 2F). This reduced MFI was likely due to the efficient cleavage of the Cy5 upon MMP2 treatment. On the contrary, if PEP_{20}-M-IFN was labeled with FAM-NHS randomly on the IFN part (denoted as PEP_{20}-M-IFN-K-FAM) as shown in Figure 2G, pre-incubation of the conjugate with the same $MMP2^+$ medium resulted in a upshifted curve and a greater MFI in flow cytometry (Figure 2H). These results suggested that the binding affinity of PEP_{20}-M-IFN was enhanced by the MMP2-triggered polymer detachment. To evaluate the in vitro antiproliferative bioactivity, cytotoxicity experiments were performed using Daudi cells. The IC_{50} values of wt-IFN, PEP_{20}-IFN, and PEP_{20}-M-IFN were 18.9, 148.2, and 76.6 pg/mL, respectively (Figure 2I). The results suggested that the activatable PEP_{20}-M-IFN was more potent than PEP_{20}-IFN against Daudi cells, likely a consequence of the polymer release during the incubation.

PKs and Biodistribution. To assess the circulation half-life, wt-IFN and the two conjugates were i.v. administered, followed by blood withdrawal at different time points. The plasma IFN levels were determined by ELISA. As shown in Figure 3A, wt-IFN was quickly cleared from blood, with an elimination half-life $t_{1/2}$-β of ~0.5 h. In contrast, both PEP_{20}-M-IFN and its noncleavable counterpart PEP_{20}-IFN had much longer half-lives (5.2 and 5.1 h, respectively).

To explore the biodistribution and intratumoral accumulation of the conjugate, the SKOV-3 tumor-bearing BALB/c-nu female mice were i.v. injected with Cy5-labeled IFN variants and then imaged at designated time points by an in vivo imaging system. Different from the previous thiol–maleimide labeled Cy5, here, the dye was randomly attached to IFN by using the NHS-amine chemistry (Figure S6). Live animal imaging of the Cy5 fluorescence suggested that the drugs were mainly cleared from liver and kidney (Figure 3B). Interestingly, the semiquantitative fluorescent imaging of the extracted tumor sections 48 h after the i.v. administration indicated that the Cy5 fluorescence of PEP_{20}-M-IFN was significantly higher and more homogeneously distributed in the entire tumor than that of PEP_{20}-IFN (Figures 3C and S7). The enhanced tumor accumulation of PEP_{20}-M-IFN was further confirmed by the more accurate anti-IFN ELISA of the homogenized tumor tissues (Figure 3D). We reasoned that the higher concentration of PEP_{20}-M-IFN over PEP_{20}-IFN in the TME was likely associated with the MMP2-mediated activation, which contributed to the higher binding affinity to the cancerous cells, and thus improved retention and decreased lymphatic clearance. To verify whether the higher tumor accumulation of PEP_{20}-M-IFN was MMP2-dependent or not,

DOI: 10.1021/acs.biomac.9b00560
Biomacromolecules 2019, 20, 3000–3008

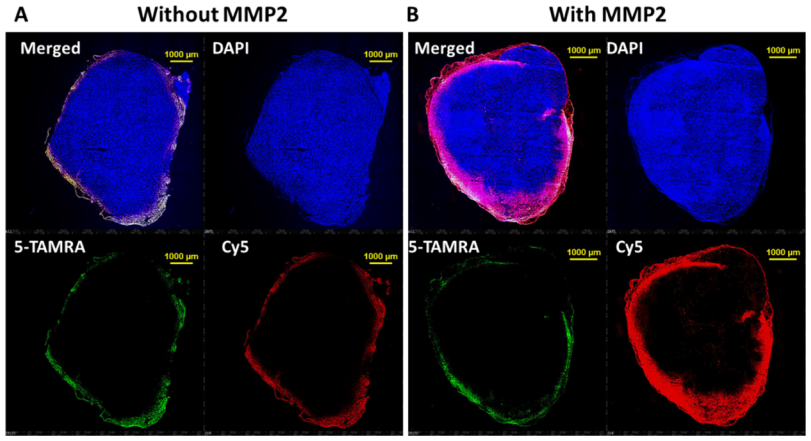

Figure 4. Ex vivo tumor penetration. The SKOV3 tumors of 50 mm^3 were cocultured with TAMRA-labeled PEP_{20}-IFN and Cy5-labeled PEP_{20}-M-IFN (0.09 mg/mL each based on IFN) in opti-MEM (A) without or (B) with supplemented MMP2 enzyme.

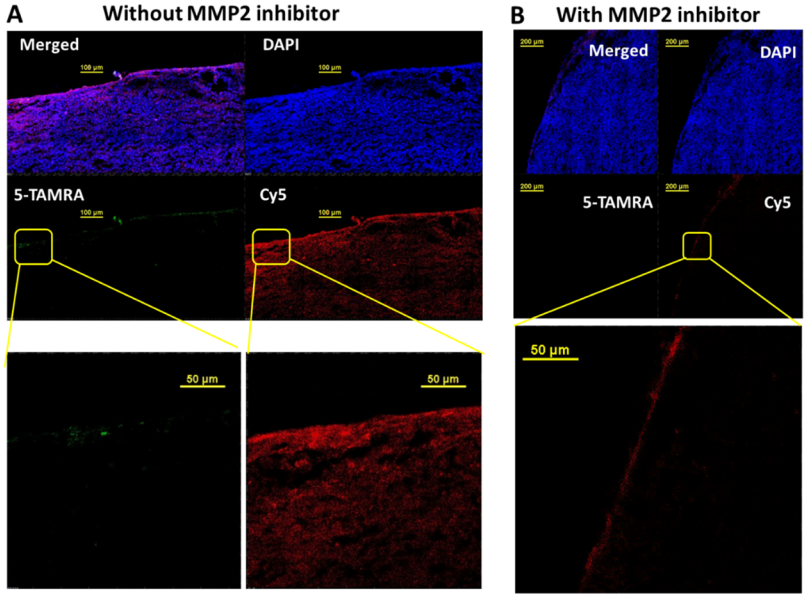

Figure 5. In vivo tumor penetration. Mice with ~200 mm^3 tumors were subcutaneously co-injected with Cy5-labeled PEP_{20}-M-IFN and TAMRA-labeled PEP_{20}-IFN (15 μg IFN for each conjugate) nearby the tumor (A) without or (B) with the intratumoral pre-injection of 1,10-phenanthroline.

the SKOV-3 tumor-bearing BALB/c-nu female mice were intratumorally injected with 1,10-phenanthroline, a zinc chelator widely used as a broad-spectrum MMP inhibitor,[61] and followed by the subcutaneous infusion of the Cy5-labeled PEP_{20}-M-IFN near the tumor site. Fluorescence intensity indicated that the degree of tumor accumulation of PEP_{20}-M-IFN was greatly reduced with the presence of 1,10-phenanthroline in the tumor (Figure 3E).

Ex Vivo and in Vivo Tumor Penetration. Next, we investigated the tumor penetration behavior of the conjugates ex vivo and in vivo. We expected that PEP_{20}-M-IFN should be able to penetrate deeper than PEP_{20}-IFN due to the significantly smaller size of the former after the MMP cleavage. For the ex vivo study, SKOV3 tumors (~50 mm^3 in size) were extracted out from mice and immersed in opti-MEM medium with or without supplemented MMP2 enzyme. TAMRA-labeled PEP_{20}-IFN and Cy5-labeled PEP_{20}-M-IFN (both randomly labeled via the NHS-amine chemistry) were co-incubated with the tumor for 24 h.[24] It was shown that both PEP_{20}-M-IFN and PEP_{20}-IFN had a similar penetration depth less than 0.2 mm without the MMP2 activation (Figure 4A, Cy5 and TAMRA). Strikingly, the penetration of PEP_{20}-M-IFN reached ~1 mm (Figure 4B, Cy5) in the $MMP2^+$ opti-MEM medium, whereas PEP_{20}-IFN still remained a relatively shallow penetration depth under the same condition (Figure 4B, TAMRA).

For the in vivo tumor penetration study, the TAMRA-labeled PEP_{20}-IFN and Cy5-labeled PEP_{20}-M-IFN were subcutaneously co-injected near the SKOV-3 tumors. After 24 h, the tumors were extracted out, sliced, stained with DAPI, and observed with confocal microscopy. Again, the penetration depth of the Cy5-labeled PEP_{20}-M-IFN reached ~1.2 mm in the tumor (Cy5 channel, Figures 5A and S8), whereas the fluorescence of 5-TAMRA labeled PEP_{20}-IFN was merely detectable at the peripheral edge of the tumor with a maximum penetration depth of 50 μm (TAMARA, Figure 5A). Furthermore, the tumor penetration of the PEP_{20}-M-IFN was significantly inhibited by the local pre-injection of the MMP inhibitor 1,10-phenanthroline to the mice (Figure 5B).

DOI: 10.1021/acs.biomac.9b00560
Biomacromolecules 2019, 20, 3000−3008

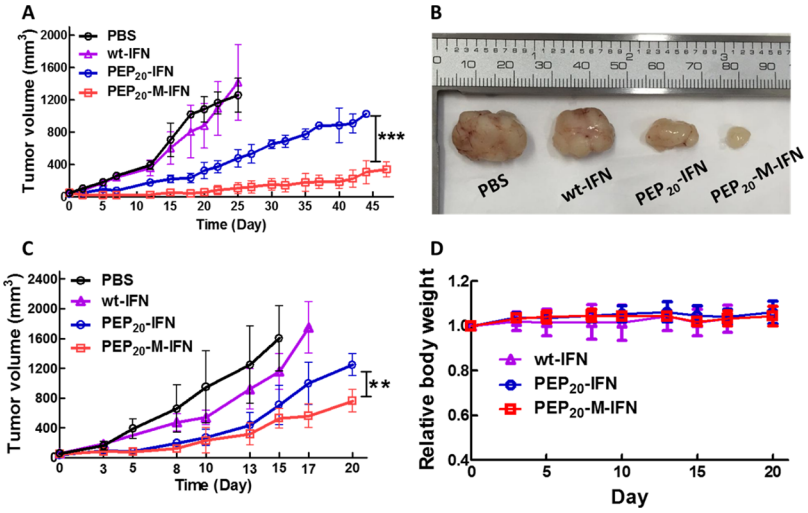

Figure 6. Antitumor efficacy of wt-IFN and the IFN conjugates. (A) Tumor growth inhibition curves and (B) photographs of the extracted OVCAR3 xenograft tumors on day 27. BALB/C-nu mice bearing s.c. OVCAR-3 tumor were i.v. injected with PBS saline, wt-IFN, PEP_{20}-IFN, or PEP_{20}-M-IFN (n = 5−7) every 5 days at a dosage of 20 μg IFN per mouse for eight times. (C) Tumor growth inhibition curve and (D) relative body weight of BALB/C-nu mice bearing s.c. SKOV-3 tumors. The mice were i.v. injected with PBS saline, wt-IFN, PEP_{20}-IFN, or PEP_{20}-M-IFN at 20 μg IFN per mouse every 5 days for four times; Data are presented as mean ± SD; *P < 0.05, **P < 0.01, ***p < 0.001 (t-test).

Together, these results demonstrated that PEP_{20}-M-IFN can reach the deep tumor tissues in a MMP2-dependent fashion.

In Vivo Efficacy. The antitumor efficacy of the conjugates was first studied in an OVCAR3 xenografts model in nude mice. When the average tumor size reached approximately 30 mm^3 (defined as day 0), mice were randomly grouped (n = 5−7) and i.v. administered with PBS, wt-IFN, PEP_{20}-IFN, or PEP_{20}-M-IFN every 5 days at a dosage of 20 μg IFN/mouse (8 injections total). As shown in Figure 6A,B, the tumor sizes grew exponentially in both wt-IFN and PBS groups, with no significant difference detected. Notably, the MMP-activatable PEP_{20}-M-IFN was found to exhibit significantly higher efficacy of tumor inhibition than its noncleavable counterpart PEP_{20}-IFN. This result underscored the necessity of both long circulation and MMP activation for suppressing the tumor growth. The superior antitumor performance of PEP_{20}-M-IFN over PEP_{20}-IFN and wt-IFN was further confirmed by hematoxylin and eosin (H&E) staining of the liver tissues (Figure S9). Compared with the healthy mice, on day 27, mice receiving wt-IFN showed severe paraneoplastic syndromes due to the infiltration of inflammatory immune cells in the liver. The PEP_{20}-IFN treatment mitigated the infiltration to some degree, but incomplete; in contrast, administration of PEP_{20}-M-IFN led to almost no lymphocyte infiltration in the liver. We further evaluated the efficacy of PEP_{20}-M-IFN in a SKOV3 xenograft model that was more aggressive than the OVCAR-3 tumors. The mice were i.v. infused with various IFN drugs by following designated regimens as described in the experimental sections. Again, PEP_{20}-M-IFN led to more pronounced tumor inhibition than the non-MMP-responsive PEP_{20}-IFN (Figure 6C). The biological safety of the IFN drugs was demonstrated by the well-maintained body weight (Figure 6D). Moreover, the conjugates showed no damage to other major tissues (e.g., kidney, spleen, lung, and heart) according to the histopathology imaging (Figure S10).

CONCLUSIONS

In summary, we report here a simple strategy harnessing the enzyme MMP in TME to achieve tissue-specific protein activation. The novel IFN conjugate PEP_{20}-M-IFN shows long circulation and slow clearance in blood due to PEPylation. In TME, PEP_{20}-M-IFN released its conjugated polymer to afford higher tumor retention, smaller size-promoted deeper tumor penetration, stronger binding, and outstanding antitumor potency in a MMP-dependent manner. Taken together, this work highlights the releasable PEPylation as a promising strategy circumventing the long-existed PEG dilemma and may open up new opportunities for malignant solid tumor treatment in clinics.

ASSOCIATED CONTENT

Supporting Information

The Supporting Information is available free of charge on the ACS Publications website at DOI: 10.1021/acs.biomac.9b00560.

ESI-MS analysis, ^{1}H NMR spectra, SEC curves, SDS-PAGE analysis, flow cytometry, fluorescence and CLSM images of organs, and histopathology evaluation (PDF)

AUTHOR INFORMATION

Corresponding Authors

*E-mail: yucaiwang@ustc.edu.cn (Y.W.).
*E-mail: chemhualu@pku.edu.cn (H.L.).

ORCID

Youqing Shen: 0000-0003-1837-7976
Yucai Wang: 0000-0001-6046-2934
Hua Lu: 0000-0003-2180-3091

Notes

The authors declare no competing financial interest.

ACKNOWLEDGMENTS

This work was financially supported by the National Key Research and Development Program of China (no. 2016YFA0201400). We thank the grants from the National Natural Science Foundation of China (21722401). H.L. thanks the startup funding from the Youth Thousand-Talents Program of China.

DOI: 10.1021/acs.biomac.9b00560
Biomacromolecules 2019, 20, 3000−3008

REFERENCES

(1) Leader, B.; Baca, Q. J.; Golan, D. E. Protein therapeutics: a summary and pharmacological classification. *Nat. Rev. Drug Discov.* **2008**, *7*, 21−39.

(2) Gu, Z.; Biswas, A.; Zhao, M.; Tang, Y. Tailoring nanocarriers for intracellular protein delivery. *Chem. Soc. Rev.* **2011**, *40*, 3638−3655.

(3) Kontos, S.; Hubbell, J. A. Drug development: longer-lived proteins. *Chem. Soc. Rev.* **2012**, *41*, 2686−2695.

(4) Walsh, G. Biopharmaceutical benchmarks 2014. *Nat. Biotechnol.* **2014**, *32*, 992−1000.

(5) Liu, X.; Wu, F.; Ji, Y.; Yin, L. Recent Advances in Anti-cancer Protein/Peptide Delivery. *Bioconjugate Chem.* **2019**, *30*, 305−324.

(6) Zhang, P.; Steinborn, B.; Lächelt, U.; Zahler, S.; Wagner, E. Lipo-Oligomer Nanoformulations for Targeted Intracellular Protein Delivery. *Biomacromolecules* **2017**, *18*, 2509−2520.

(7) Chen, M.-C.; Mi, F.-L.; Liao, Z.-X.; Hsiao, C.-W.; Sonaje, K.; Chung, M.-F.; Hsu, L.-W.; Sung, H.-W. Recent advances in chitosan-based nanoparticles for oral delivery of macromolecules. *Adv. Drug Delivery Rev.* **2013**, *65*, 865−879.

(8) He, Z.; Santos, J. L.; Tian, H.; Huang, H.; Hu, Y.; Liu, L.; Leong, K. W.; Chen, Y.; Mao, H.-Q. Scalable fabrication of size-controlled chitosan nanoparticles for oral delivery of insulin. *Biomaterials* **2017**, *130*, 28−41.

(9) He, C.; Tang, Z.; Tian, H.; Chen, X. Co-delivery of chemotherapeutics and proteins for synergistic therapy. *Adv. Drug Delivery Rev.* **2016**, *98*, 64−76.

(10) Pelegri-O'Day, E. M.; Lin, E. W.; Maynard, H. D. Therapeutic protein-polymer conjugates: advancing beyond PEGylation. *J. Am. Chem. Soc.* **2014**, *136*, 14323−14332.

(11) Liu, X.; Sun, J.; Gao, W. Site-selective protein modification with polymers for advanced biomedical applications. *Biomaterials* **2018**, *178*, 413−434.

(12) Wu, Y.; Ng, D. Y. W.; Kuan, S. L.; Weil, T. Protein-polymer therapeutics: a macromolecular perspective. *Biomater. Sci.* **2015**, *3*, 214−230.

(13) Huang, A.; Qin, G.; Olsen, B. D. Highly Active Biocatalytic Coatings from Protein-Polymer Diblock Copolymers. *ACS Appl. Mater. Interfaces* **2015**, *7*, 14660−14669.

(14) Zhang, P.; Sun, F.; Tsao, C.; Liu, S.; Jain, P.; Sinclair, A.; Hung, H.-C.; Bai, T.; Wu, K.; Jiang, S. Zwitterionic gel encapsulation promotes protein stability, enhances pharmacokinetics, and reduces immunogenicity. *Proc. Natl. Acad. Sci. U.S.A.* **2015**, *112*, 12046−12051.

(15) Fuhrmann, G.; Grotzky, A.; Lukić, R.; Matoori, S.; Luciani, P.; Yu, H.; Zhang, B.; Walde, P.; Schlüter, A. D.; Gauthier, M. A.; Leroux, J.-C. Sustained gastrointestinal activity of dendronized polymer-enzyme conjugates. *Nat. Chem.* **2013**, *5*, 582−589.

(16) Gao, W.; Liu, W.; Christensen, T.; Zalutsky, M. R.; Chilkoti, A. In situ growth of a PEG-like polymer from the C terminus of an intein fusion protein improves pharmacokinetics and tumor accumulation. *Proc. Natl. Acad. Sci. U.S.A.* **2010**, *107*, 16432−16437.

(17) Russell, A. J.; Baker, S. L.; Colina, C. M.; Figg, C. A.; Kaar, J. L.; Matyjaszewski, K.; Simakova, A.; Sumerlin, B. S. Next generation protein-polymer conjugates. *AIChE J.* **2018**, *64*, 3230−3245.

(18) Hatakeyama, H.; Akita, H.; Harashima, H. The Polyethyleneglycol Dilemma: Advantage and Disadvantage of PEGylation of Liposomes for Systemic Genes and Nucleic Acids Delivery to Tumors. *Biol. Pharm. Bull.* **2013**, *36*, 892−899.

(19) Chen, Y.; Zhang, M.; Jin, H.; Tang, Y.; Wang, H.; Xu, Q.; Li, Y.; Li, F.; Huang, Y. Intein-mediated site-specific synthesis of tumor-targeting protein delivery system: Turning PEG dilemma into prodrug-like feature. *Biomaterials* **2017**, *116*, 57−68.

(20) Keefe, A. J.; Jiang, S. Poly(zwitterionic)protein conjugates offer increased stability without sacrificing binding affinity or bioactivity. *Nat. Chem.* **2011**, *4*, 59−63.

(21) Bailon, P.; Palleroni, A.; Schaffer, C. A.; Spence, C. L.; Fung, W.-J.; Porter, J. E.; Ehrlich, G. K.; Pan, W.; Xu, Z.-X.; Modi, M. W.; Farid, A.; Berthold, W.; Graves, M. Rational Design of a Potent, Long-Lasting Form of Interferon: A 40 kDa Branched Polyethylene Glycol-Conjugated Interferon α-2a for the Treatment of Hepatitis C. *Bioconjugate Chem.* **2001**, *12*, 195−202.

(22) Fishburn, C. S. The pharmacology of PEGylation: balancing PD with PK to generate novel therapeutics. *J. Pharm. Sci.* **2008**, *97*, 4167−4183.

(23) Hou, Y.; Yuan, J.; Zhou, Y.; Yu, J.; Lu, H. A Concise Approach to Site-Specific Topological Protein-Poly(Amino Acid) Conjugates Enabled by In-situ Generated Functionalities. *J. Am. Chem. Soc.* **2016**, *138*, 10995−11000.

(24) Hou, Y.; Zhou, Y.; Wang, H.; Wang, R.; Yuan, J.; Hu, Y.; Sheng, K.; Feng, J.; Yang, S.; Lu, H. Macrocyclization of Interferon-Poly(α-amino acid) Conjugates Significantly Improves the Tumor Retention, Penetration, and Antitumor Efficacy. *J. Am. Chem. Soc.* **2018**, *140*, 1170−1178.

(25) Hu, Y.; Hou, Y.; Wang, H.; Lu, H. Polysarcosine as an Alternative to PEG for Therapeutic Protein Conjugation. *Bioconjugate Chem.* **2018**, *29*, 2232−2238.

(26) Yuan, J.; Sun, Y.; Wang, J.; Lu, H. Phenyl Trimethylsilyl Sulfide-Mediated Controlled Ring-Opening Polymerization of α-Amino Acid N-Carboxyanhydrides. *Biomacromolecules* **2016**, *17*, 891−896.

(27) Zhang, C.; Lu, H. Efficient Synthesis and Application of Protein-Poly(α-amino acid) Conjugates. *Acta Polym. Sin.* **2018**, *1*, 21−31.

(28) Deming, T. J. Synthesis of Side-Chain Modified Polypeptides. *Chem. Rev.* **2016**, *116*, 786−808.

(29) Song, Z.; Fu, H.; Wang, R.; Pacheco, L. A.; Wang, X.; Lin, Y.; Cheng, J. Secondary structures in synthetic polypeptides from N-carboxyanhydrides: design, modulation, association, and material applications. *Chem. Soc. Rev.* **2018**, *47*, 7401−7425.

(30) Birke, A.; Ling, J.; Barz, M. Polysarcosine-containing copolymers: Synthesis, characterization, self-assembly, and applications. *Prog. Polym. Sci.* **2018**, *81*, 163−208.

(31) Mochida, Y.; Cabral, H.; Miura, Y.; Albertini, F.; Fukushima, S.; Osada, K.; Nishiyama, N.; Kataoka, K. Bundled assembly of helical nanostructures in polymeric micelles loaded with platinum drugs enhancing therapeutic efficiency against pancreatic tumor. *ACS Nano* **2014**, *8*, 6724−6738.

(32) Deng, C.; Wu, J.; Cheng, R.; Meng, F.; Klok, H.-A.; Zhong, Z. Functional polypeptide and hybrid materials: Precision synthesis via α -amino acid N -carboxyanhydride polymerization and emerging biomedical applications. *Prog. Polym. Sci.* **2014**, *39*, 330−364.

(33) Shen, Y.; Fu, X.; Fu, W.; Li, Z. Biodegradable stimuli-responsive polypeptide materials prepared by ring opening polymerization. *Chem. Soc. Rev.* **2015**, *44*, 612−622.

(34) Chen, J.; Ding, J.; Wang, Y.; Cheng, J.; Ji, S.; Zhuang, X.; Chen, X. Sequentially Responsive Shell-Stacked Nanoparticles for Deep Penetration into Solid Tumors. *Adv. Mater.* **2017**, *29*, 1701170.

(35) Duro-Castano, A.; Nebot, V. J.; Niño-Pariente, A.; Armiñán, A.; Arroyo-Crespo, J. J.; Paul, A.; Feiner-Gracia, N.; Albertazzi, L.; Vicent, M. J. Capturing "Extraordinary" Soft-Assembled Charge-Like Polypeptides as a Strategy for Nanocarrier Design. *Adv. Mater.* **2017**, *29*, 1702888.

(36) Miao, Y.; Xie, F.; Cen, J.; Zhou, F.; Tao, X.; Luo, J.; Han, G.; Kong, X.; Yang, X.; Sun, J.; Ling, J. Fe3+@polyDOPA-b-polysarcosine, a T1-Weighted MRI Contrast Agent via Controlled NTA Polymerization. *ACS Macro Lett.* **2018**, *7*, 693−698.

(37) Rodríguez-Hernández, J.; Lecommandoux, S. Reversible Inside−Out Micellization of pH-responsive and Water-Soluble Vesicles Based on Polypeptide Diblock Copolymers. *J. Am. Chem. Soc.* **2005**, *127*, 2026−2027.

(38) Hou, Y.; Zhou, Y.; Wang, H.; Sun, J.; Wang, R.; Sheng, K.; Yuan, J.; Hu, Y.; Chao, Y.; Liu, Z.; Lu, H. Therapeutic Protein PEPylation: The Helix of Nonfouling Synthetic Polypeptides Minimizes Antidrug Antibody Generation. *ACS Cent. Sci.* **2019**, *5*, 229−236.

(39) Gong, Y.; Leroux, J.-C.; Gauthier, M. A. Releasable conjugation of polymers to proteins. *Bioconjugate Chem.* **2015**, *26*, 1172−1181.

DOI: 10.1021/acs.biomac.9b00560
Biomacromolecules 2019, 20, 3000−3008

(40) Chen, J.; Zhao, M.; Feng, F.; Sizovs, A.; Wang, J. Tunable thioesters as "reduction" responsive functionality for traceless reversible protein PEGylation. *J. Am. Chem. Soc.* **2013**, *135*, 10938−10941.
(41) Ferguson, E. L.; Duncan, R. Dextrin-phospholipase A2: synthesis and evaluation as a bioresponsive anticancer conjugate. *Biomacromolecules* **2009**, *10*, 1358−1364.
(42) Wang, M.; Sun, S.; Neufeld, C. I.; Perezramirez, B.; Xu, Q. Reactive oxygen species-responsive protein modification and its intracellular delivery for targeted cancer therapy. *Angew. Chem., Int. Ed.* **2014**, *53*, 13444−13448.
(43) Qian, L.; Fu, J.; Yuan, P.; Du, S.; Huang, W.; Li, L.; Yao, S. Q. Intracellular Delivery of Native Proteins Facilitated by Cell-Penetrating Poly(disulfide)s. *Angew. Chem., Int. Ed.* **2018**, *57*, 1532−1536.
(44) Zhu, Q.; Chen, X.; Xu, X.; Zhang, Y.; Zhang, C.; Mo, R. Tumor-Specific Self-Degradable Nanogels as Potential Carriers for Systemic Delivery of Anticancer Proteins. *Adv. Funct. Mater.* **2018**, *28*, 1707371.
(45) Roy, R.; Yang, J.; Moses, M. A. Matrix metalloproteinases as novel biomarkers and potential therapeutic targets in human cancer. *J. Clin. Oncol.* **2009**, *27*, 5287−5297.
(46) Egeblad, M.; Werb, Z. New functions for the matrix metalloproteinases in cancer progression. *Nat. Rev. Cancer* **2002**, *2*, 161−174.
(47) Zhu, L.; Wang, T.; Perche, F.; Taigind, A.; Torchilin, V. P. Enhanced anticancer activity of nanopreparation containing an MMP2-sensitive PEG-drug conjugate and cell-penetrating moiety. *Proc. Natl. Acad. Sci. U.S.A.* **2013**, *110*, 17047−17052.
(48) Liu, Y.; Zhang, D.; Qiao, Z.-Y.; Qi, G.-B.; Liang, X.-J.; Chen, X.-G.; Wang, H. A Peptide-Network Weaved Nanoplatform with Tumor Microenvironment Responsiveness and Deep Tissue Penetration Capability for Cancer Therapy. *Adv. Mater.* **2015**, *27*, 5034−5042.
(49) Peng, Z.-H.; Kopeček, J. Enhancing Accumulation and Penetration of HPMA Copolymer-Doxorubicin Conjugates in 2D and 3D Prostate Cancer Cells via iRGD Conjugation with an MMP-2 Cleavable Spacer. *J. Am. Chem. Soc.* **2015**, *137*, 6726−6729.
(50) Jiang, T.; Olson, E. S.; Nguyen, Q. T.; Roy, M.; Jennings, P. A.; Tsien, R. Y. Tumor imaging by means of proteolytic activation of cell-penetrating peptides. *Proc. Natl. Acad. Sci. U.S.A.* **2004**, *101*, 17867−17872.
(51) Choi, K. Y.; Swierczewska, M.; Lee, S.; Chen, X. Protease-activated drug development. *Theranostics* **2012**, *2*, 156−179.
(52) Li, Y.; Li, W.; Bao, W.; Liu, B.; Li, D.; Jiang, Y.; Wei, W.; Ren, F. Bioinspired peptosomes with programmed stimuli-responses for sequential drug release and high-performance anticancer therapy. *Nanoscale* **2017**, *9*, 9317−9324.
(53) Li, Y.; Xu, X.; Zhang, X.; Li, Y.; Zhang, Z.; Gu, Z. Tumor-Specific Multiple Stimuli-Activated Dendrimeric Nanoassemblies with Metabolic Blockade Surmount Chemotherapy Resistance. *ACS Nano* **2017**, *11*, 416−429.
(54) Zhang, J.; Yuan, Z.-F.; Wang, Y.; Chen, W.-H.; Luo, G.-F.; Cheng, S.-X.; Zhuo, R.-X.; Zhang, X.-Z. Multifunctional Envelope-Type Mesoporous Silica Nanoparticles for Tumor-Triggered Targeting Drug Delivery. *J. Am. Chem. Soc.* **2013**, *135*, 5068−5073.
(55) Dudani, J. S.; Buss, C. G.; Akana, R. T. K.; Kwong, G. A.; Bhatia, S. N. Sustained-Release Synthetic Biomarkers for Monitoring Thrombosis and Inflammation Using Point-of-Care Compatible Readouts. *Adv. Funct. Mater.* **2016**, *26*, 2919−2928.
(56) Braun, A. C.; Gutmann, M.; Mueller, T. D.; Lühmann, T.; Meinel, L. Bioresponsive release of insulin-like growth factor-I from its PEGylated conjugate. *J. Control. Release* **2018**, *279*, 17−28.
(57) Li, H.-J.; Du, J.-Z.; Du, X.-J.; Xu, C.-F.; Sun, C.-Y.; Wang, H.-X.; Cao, Z.-T.; Yang, X.-Z.; Zhu, Y.-H.; Nie, S.; Wang, J. Stimuli-responsive clustered nanoparticles for improved tumor penetration and therapeutic efficacy. *Proc. Natl. Acad. Sci. U.S.A.* **2016**, *113*, 4164−4169.
(58) Li, L.; Sun, W.; Zhong, J.; Yang, Q.; Zhu, X.; Zhou, Z.; Zhang, Z.; Huang, Y. Multistage Nanovehicle Delivery System Based on Stepwise Size Reduction and Charge Reversal for Programmed Nuclear Targeting of Systemically Administered Anticancer Drugs. *Adv. Funct. Mater.* **2015**, *25*, 4101−4113.
(59) Wong, C.; Stylianopoulos, T.; Cui, J.; Martin, J.; Chauhan, V. P.; Jiang, W.; Popovic, Z.; Jain, R. K.; Bawendi, M. G.; Fukumura, D. Multistage nanoparticle delivery system for deep penetration into tumor tissue. *Proc. Natl. Acad. Sci. U.S.A.* **2011**, *108*, 2426−2431.
(60) Tsvetkova, Y.; Beztsinna, N.; Baues, M.; Klein, D.; Rix, A.; Golombek, S. K.; Al Rawashdeh, W. e.; Gremse, F.; Barz, M.; Koynov, K.; Banala, S.; Lederle, W.; Lammers, T.; Kiessling, F. Balancing Passive and Active Targeting to Different Tumor Compartments Using Riboflavin-Functionalized Polymeric Nanocarriers. *Nano Lett.* **2017**, *17*, 4665−4674.
(61) Bremer, C.; Tung, C.-H.; Weissleder, R. In vivo molecular target assessment of matrix metalloproteinase inhibition. *Nat. Med.* **2001**, *7*, 743−748.

DOI: 10.1021/acs.biomac.9b00560
Biomacromolecules 2019, 20, 3000−3008